Beam Centric Doppler Pre-Compensation for LEO-based 5G-NTN

Ashish Kumar Meshram, Sumit Kumar, Jorge Querol, Symeon Chatzinotas
Interdisciplinary Centre for Security, Reliability and Trust (SnT), University of Luxembourg, Luxembourg
Email:{ashish.meshram, sumit.kumar, jorge.querol,symeon.chatzinotas}@uni.lu,

***Abstract*—Integration of Non-Terrestrial Networks (NTN) components with 5G Terrestrial Networks (TN) is getting significant traction from academia and industry, resulting in the standardization of 5G-NTN in 3GPP. Low Earth Orbit (LEO) based 5G-NTN, especially regenerative payload, are of particular interest as they can provide latency and throughput comparable to terrestrial 5G networks. Initial synchronization is the first step when a User Equipment (UE) attempts to establish a data link with the gNB. However, the excessive Doppler caused by the LEO satellite's fast movement must be exclusively compensated before the UE can successfully align time and frequency. This work presents an effective method to address this issue. In this method, a regenerative LEO satellite-based 5G gNodeB (gNB) pre-compensates the Doppler with respect to its Beam Center (BC) before any transmission. Further, a UE post-compensates the residual Doppler to achieve successful initial synchronization. With the proposed methodology, we expect the accuracy of initial synchronization to be comparable to 5G-TN without increasing the processing complexity at the UE. Furthermore, for the realistic scenario, our analysis includes the effect of the LEO satellite trajectory error sphere and pointing error.**

***Index Terms*—5G New Radio, Non-Terrestrial Networks, Trajectory Error Sphere, Beam Pointing Error, Estimation, Doppler Shift, Compensation, Initial Synchronization**

I. Introduction

Introducing satellite components in the recent 3GPP Release-17 has accelerated the long-awaited convergence of 5G and beyond 5G TN and NTN [1], [2]. The 5G-NR protocol stack, initially designed for TN, has been selected as the technology for 5G-NTN due to its distinctive physical layer characteristics. However, integrating 5G-TN with NTN components presents complex challenges, particularly considering the effects of the high mobility of LEO satellites which cause significantly high Doppler [3]. This results in a mismatch of the Carrier Frequency Offset (CFO) between the transmitter and receiver, further increasing Inter-Carrier Interference (ICI) [4] leading to difficulties in achieving initial synchronization. Furthermore, it imposes higher complexity on receiver-side algorithms to estimate and compensate CFO and ICI. While having prior information about the satellite orbits would mitigate this challenge with a trade-off in overhead and frequent updation, obtaining such information about the regenerative satellite orbits at the UE before initial synchronization is challenging due to the dynamicity of LEO satellites, limited visibility duration, time synchronization, and ephemeris data volume constraints [5].

Most of the past works that have addressed the Doppler effects for 5G-NTN can be categorized under Doppler characterization, propagation impairment in the LEO satellite channel, and Multple-Input Multiple-Output (MIMO). We emphasize some noteworthy solutions available and their limitations. In [6]–[12], Doppler frequency characterization relies on the two-body equation of motion without considering the effect of the satellite orbital perturbation, which can cause satellites to drift from their intended positions, affecting their ability to maintain accurate and stable communications. In [13], the Doppler shift is expressed in terms of the Taylor series up to the second term consisting of the Doppler shift and rate. The high non-linearity of the Doppler shift function poses a challenge when using a limited number of terms in the Taylor series approximation can lead to significant errors for large frequency deviations or rapid changes. Whereas [14]–[16], do not consider any prior information on Doppler characterization resulting in complex estimation and compensation algorithm at the UE. Specifically, [16] proposes an additional 5G NR Synchronization Signal Block (SSB) placement in different frequency locations, resulting in further overhead. In terms of propagation channel, most studies focus on multipath channels [7], [11], [12], [14] but fail to address the impact of large-scale fading caused by the large distance between the satellite and ground UE. This effect varies depending on the location of the UE, whether it is in densely populated or rural areas. When considering MIMO, it is essential to mention that no analytical work has been done so far, apart from the study by [16], which focused on a simulation involving a UE with two receive antennas.

We also mention two recent experimental projects, 5G-GOA [17], and 5G-LEO [18] where open-source based Software Defined Radio (SDR) framework OpenAirInterface5G has been used for over-the-satellite real-world experiments. 5G-GOA addresses challenges caused by significant delay (approx 520ms) and does not focus on Doppler. While 5G-LEO addresses the Doppler, it considers only transparent payload satellites. Moreover, 5G-LEO does not provide an analytical approach to compensate for the Doppler.

Considering the limitations mentioned above, our contributions to this work as listed below:

1. We propose a model for the satellite orbital trajectory sphere, accounting for inaccuracies in satellite position vectors and beam pointing errors in the pre-compensation of Doppler frequency.
2. An efficient method for Doppler frequency pre-compensation at the satellite to reduce the complexity of the UE CFO estimation algorithm, where the UE does not need apriori knowledge of the satellite's ephemeris during the initial synchronization phase.
3. Finally, we provide an efficient algorithm for estimating frequency offset in the time domain, which uses Cyclic Prefix (CP) based correlation and works satisfactorily even on low Signal-to-Noise Ratio (SNR).

Throughout this paper, we follow these notations unless specified specifically: $c = 3 \times 10^8$ (m/s) for the speed of light. Small and capital boldface symbol $\mathbf{x}, \mathbf{X}$ for complex-valued IQ samples in time- and frequency-domain, respectively. $\circledast$ for convolution and $*$ for conjugation operations, respectively. $\mathcal{N}(\mu, \sigma^2)$ represents Normally distributed random numbers with μ mean and σ^2 variance. Probability is denoted as $\Pr(\cdot)$, $\mathbb{E}[\cdot], \mathbb{V}\text{ar}[\cdot]$ for expectation and variance operation, $f_{\text{X}}(x), F_{\text{X}}(x)$ for probability and cumulative distribution function of a random variable X, respectively. Furthermore, mathematical steps in obtaining final expressions have been omitted for brevity.

II. System Model

Our system model considers a scenario with a regenerative payload LEO satellite equipped with steerable spot beams fixed to the specific location on the Earth's surface, as shown in Fig. 1. During its orbital journey, a satellite encounters perturbing influences like atmospheric drag, solar radiation pressure, Earth's oblateness, and the gravitational effects of celestial bodies beyond Earth. To accommodate these factors, we model a satellite trajectory sphere—a spatial domain delineating the projected satellite location at a specific instant. This sphere considers the imprecisions in the satellite position vector. Let $\tilde{\mathbf{r}}_{\text{sat}}$ the satellite ideal position vector in Earth-Centered, Earth-Fixed (ECEF) coordinates system at a given time instant, and $\mathcal{N}(\mu_{\ell,\text{sat}}, \sigma^2_{\ell,\text{sat}}), \ell \in \{x, y, z\}$ denotes the imprecisions in the satellite position vector with respect to satellite position. Furthermore, the spot beam on the satellite possesses information about its designated location on the Earth's surface where the beam has to point, known as the beam center (BC). Let $(\tilde{\phi}_{\text{BC}}, \tilde{\lambda}_{\text{BC}})$ represent the latitude and longitude and $\tilde{\mathbf{r}}_{\text{BC}} \in \mathbb{R}^3$ in ECEF coordinates system denotes the BC position vector, respectively. In an ideal situation, this knowledge enables the satellite to precisely direct its spot beams towards specific points on Earth as it moves along its orbit. However, due to orbital perturbations, onboard attitude control and position determination errors, the satellite can introduce an error while pointing toward the BC, assuming an error to be modeled as $\mathcal{N}(\mu_{\theta_{\text{pc}}}, \sigma^2_{\theta_{\text{pc}}})$. Besides these, we assume that the onboard transmitter is equipped with N_{TX} number of transmit antenna, with a transmitting power P_{TX}. The UE is equipped with N_{RX} number of receive antenna. Furthermore, UE does not have apriori information about the satellite ephemeris. Nevertheless, neither the satellite nor the UE initially knows the location of each other before synchronization.

A. Channel Model

We consider a quasi-static frequency-selective channel model, where $\mathbf{h}_p^{(i,j)}(t, \tau) \in \mathbb{C}^{N_{\text{RX}} \times N_{\text{TX}}}$ denotes the channel impulse response for the p-th UE as

$$\mathbf{h}_p^{(i,j)}(t, \tau) = \sqrt{\mathcal{P}_p} \sum_{q=0}^{Q_p - 1} \alpha_{p,q}^{(i,j)} e^{j2\pi\epsilon_{\text{D,p}}\Delta f t} \delta(\tau - \tau_{p,q}), \quad (1)$$

where $i \in \{0, 1, \cdots, N_{\text{RX}} - 1\}, j \in \{0, 1, \cdots, N_{\text{TX}} - 1\}$, $\mathcal{P}_p = 10^{-(\mathcal{P}_{\text{d}} + \mathcal{P}_{\text{S}})/10}$, $\mathcal{P}_{\text{d}} = 20 \log_{10}(4\pi d f_c / c)$ represents the large scale fading loss due to distance d between the satellite and p-th UE, $\mathcal{P}_{\text{S}} \sim \mathcal{N}(0, \sigma_S^2)$ represents the shadowing with

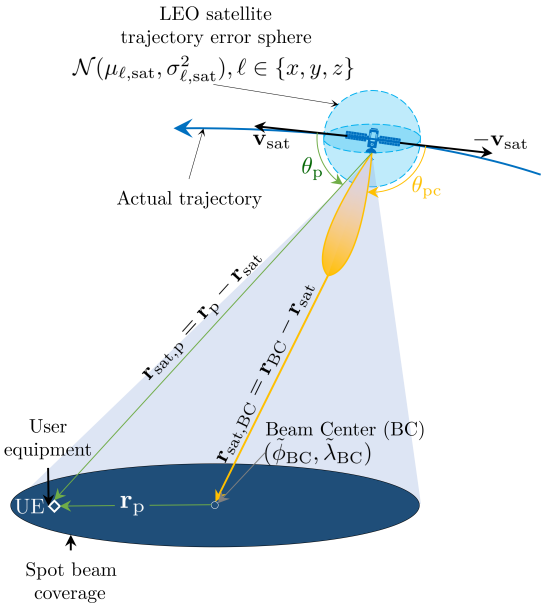

Fig. 1: Schematic of the system model, where $\mathbf{r}_{\text{BC}}, \mathbf{r}_{\text{p}}, \mathbf{r}_{\text{sat}}$ are the relative position vector of the BC, UE, and satellite with respect to Earth. And $\mathbf{v}_{\text{sat}}$ is relative velocity vector of the satellite with respect to Earth.

σ_S^2 variance. Whereas $q, Q_p, \alpha_{p,q}, \tau_{p,q}$ represents the index of the path, the total number of paths, small-scale path gain and delay for the p-th UE and qth path according to NTN-TDL-D [19], respectively. Furthermore, $\epsilon_{\text{D,p}} = f_{\text{D,p}}/\Delta f$, is the normalized Doppler frequency with respect to OFDM Sub-Carrier-Spacing (SCS) denoted as Δf. $f_{\text{D,p}}$ Doppler frequency resulting due to motion of satellite and UE. The assumption of the quasi-static channel that does not vary between the slots is justifiable due to the duration of the 5G NR slot [20]. Furthermore, the Doppler frequency at the p-th UE location can be expressed as $f_{\text{D,p}} = (v_{\text{p,sat}}/c) f_c \cos\theta_{\text{p}}$, where $\mathbf{v}_{\text{p,sat}} = \mathbf{v}_{\text{sat}} - \mathbf{v}_{\text{p}}$ is the relative velocity vector between the UE and satellite, $v_{\text{p,sat}} = |\mathbf{v}_{\text{p,sat}}|$ is the magnitude of relative velocity vector, $\mathbf{r}_{\text{sat,p}} = \mathbf{r}_{\text{p}} - \mathbf{r}_{\text{sat}}$ is the relative position vector between the satellite and UE, and $|\mathbf{r}_{\text{sat,p}}|$ is the magnitude of relative position vector. Whereas θ_{p} is angle between the direction of arrival of signal and the relative velocity vector, given as

$$\theta_{\text{p}} = \cos^{-1} \frac{\mathbf{v}_{\text{p,sat}} \cdot \mathbf{r}_{\text{sat,p}}}{|\mathbf{v}_{\text{p,sat}}||\mathbf{r}_{\text{sat,p}}|}, \quad (2)$$

B. Satellite Transmitter Signal Model

We consider an OFDM signal supporting multiple SCS. The OFDM baseband equivalent model of the transmit signal can then be expressed as

$$\tilde{\mathbf{x}}[n] = \frac{1}{N} \sum_{k=0}^{N-1} \mathbf{X}[k] e^{j2\pi r n/N}. \quad (3)$$

For $n = -N_{\text{CP}}, \cdots, N-1$. Where $N, N_{\text{CP}}, \mathbf{X}[k]$ denotes FFT size, length of cyclic prefix, the rth sub-carrier symbol.

Doppler Pre-Compensated Signal: The satellite applies Doppler frequency pre-compensation to the OFDM signal before transmission, considering the BC location on Earth.

The pre-compensated signal can be expressed mathematically using (3) as

$$\begin{aligned}\mathbf{x}[n] &= \tilde{\mathbf{x}}[n]e^{\jmath 2\pi r\epsilon^{\mathrm{pc}}_{\mathrm{D,sat}}n/N} \\ &= \frac{1}{N}\sum_{k=0}^{N-1}\mathbf{X}[k]e^{\jmath 2\pi(r+\epsilon^{\mathrm{pc}}_{\mathrm{D,sat}})n/N},\end{aligned} \tag{4}$$

where $\epsilon^{\mathrm{pc}}_{\mathrm{D,sat}} = f^{\mathrm{pc}}_{\mathrm{D,sat}}/\Delta f$ is the pre-compensated normalized Doppler frequency, and $f^{\mathrm{pc}}_{\mathrm{D,sat}} = (v_{\mathrm{sat}}/c)f_c\cos\theta_{\mathrm{pc}}$, where θ_{pc} is the angle between the transmitted signal direction towards the BC and the negative of satellite velocity vector expressed as

$$\theta_{\mathrm{pc}} = \cos^{-1}\frac{-\mathbf{v}_{\mathrm{sat}}\cdot\mathbf{r}_{\mathrm{sat,BC}}}{|\mathbf{v}_{\mathrm{sat}}||\mathbf{r}_{\mathrm{sat,BC}}|}, \tag{5}$$

where $v_{\mathrm{sat}} = |\mathbf{v}_{\mathrm{sat}}|, \mathbf{v}_{\mathrm{sat}}, r_{\mathrm{sat,BC}} = |\mathbf{r}_{\mathrm{sat,BC}}|, \mathbf{r}_{\mathrm{sat,BC}} = \mathbf{r}_{\mathrm{BC}} - \mathbf{r}_{\mathrm{sat}}$ is the magnitude of satellite velocity vector, satellite velocity vector and the relative position vector between the satellite and beam-center respectively. As shown in Fig. 2, the

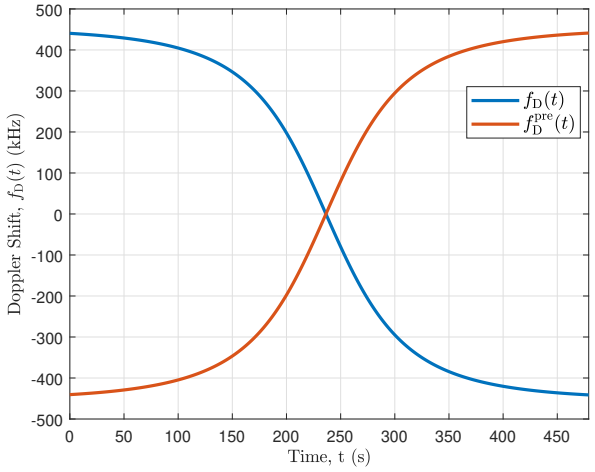

Fig. 2: Doppler frequency curve and satellite pre-compensated Doppler frequency

pre-compensated Doppler frequency complements the actual Doppler frequency. So, the residual Doppler frequency at the BC will be zero in an ideal situation.

C. User Terminal Received Signal Model

The downlink received signal at the i-th receive antenna of the p-th UE at the n-th discrete time instant can be expressed as

$$\begin{aligned}\mathbf{y}^{(i)}_p[n] &= \sum_{j=0}^{N_T-1}\left(\mathbf{h}^{(i,j)}_p(n,m)\circledast\mathbf{x}^{(j)}[n]\right) + \mathbf{w}^{(i)}_p[n] \\ &= \sum_{j=0}^{N_T-1}\sqrt{\mathcal{P}_p}\sum_{q=0}^{Q_p-1}\alpha^{(i,j)}_{p,q}e^{\jmath 2\pi\epsilon_{\mathrm{D,p}}n/N} \\ &\times\mathbf{x}^{(j)}[n-m_{p,q}] + \mathbf{w}^{(i)}_p[n],\end{aligned} \tag{6}$$

where $\mathbf{h}^{(i,j)}_p(n,m)$ represents the discrete-time channel impulse response of (1) and $\mathbf{w}^{(i)}_p[n] \sim \mathcal{CN}(0,\sigma^2_w)$ is the complex white Gaussian noise modeled as complex Gaussian random variable with zero mean and variance σ^2_w. Whereas in the frequency domain, the received symbols can be expressed as

$$\begin{aligned}\mathbf{Y}^{(i)}_p[k] &= \sum_{n=0}^{N-1}\mathbf{y}^{(i)}_p[n]e^{-\jmath 2\pi kn/N} \\ &= \sum_{j=0}^{N_T-1}\frac{1}{N}\sum_{r=0}^{N-1}\mathbf{X}^{(j)}[r]e^{-\jmath 2\pi(r+\epsilon^{\mathrm{pc}}_{\mathrm{D,sat}})m_{p,q}/N} \\ &\times\sqrt{\mathcal{P}_p}\sum_{q=0}^{Q_p-1}\alpha^{(i,j)}_{p,q}e^{\jmath\pi(r-k+\epsilon^{\mathrm{res}})(1-1/N)} \\ &\times\frac{\sin\{\pi(r-k+\epsilon^{\mathrm{res}})\}}{\sin\{\pi(r-k+\epsilon^{\mathrm{res}})/N\}} + \mathbf{W}^{(i)}_p[k],\end{aligned} \tag{7}$$

where in (7)

$$\epsilon^{\mathrm{res}} = \epsilon^{\mathrm{pc}}_{\mathrm{D,sat}} + \epsilon_{\mathrm{D,p}}, \tag{8}$$

is the normalized residual frequency. In case of flat fading with a single transmit and receive antenna (7) will be equivalent to [4].

III. Estimation, Post Compensation, and Detection

The UE will observe the residual frequency (7) at a distance d from the BC, which requires its estimation before post-compensation for proper synchronization. And since we want to assess the pre-compensation techniques, we assume that the UE is stationary and has a negligible CFO due to imperfection in the crystal oscillator. Thus we rely on the estimation of residual frequency using CP, [21] from multiple symbols in a 5G slot i.e.

$$\hat{f}_0 = -\frac{\angle\{\mathbb{E}[\mathbf{y}_p[n]\mathbf{y}^*_p[n+N]]\}}{2\pi NT_s}, \tag{9}$$

where T_s is the sampling time and $\hat{f}_0$ is bounded within $\pm\Delta f/2$ [21]. However, correct estimation using (9) requires detecting the location of CP in an OFDM symbol for which we provide an Algorithm. During the detection of CP location, there will be the possibility of false detection. This situation arises when $\mathbf{y}_p[n]$ and $\mathbf{y}_p[n+N]$ consists of noise. So we compute a threshold for the desired probability of false detection P_{FA}. Our simulation verified that the expression in step 7 of Algorithm follows the Rayleigh distribution. Thus for the desired P_{FA}, the threshold can be expressed as,

$$\beta_{\mathrm{CP}} = \sqrt{-2\eta\ln P_{\mathrm{FA}}}, \tag{10}$$

where η is the Rayleigh parameter, which can be evaluated using the Maximum Likelihood estimation as (11)

$$\eta = \frac{1}{2N}\sum_{l=0}^{N-1}\rho^2[l]. \tag{11}$$

After estimating the residual Doppler frequency, we can express the compensation of the received signal as (12).

$$\mathbf{y}^{(i)}_{c,p}[n] = \mathbf{y}^{(i)}_p[n]e^{-\jmath 2\pi\hat{f}_0 n}. \tag{12}$$

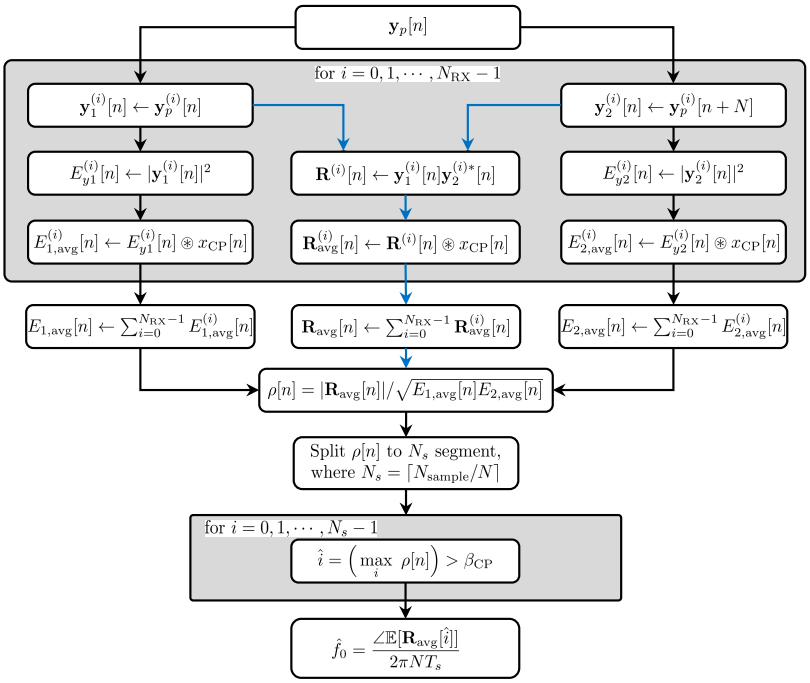

Fig. 3: Algorithm for residual Doppler frequency estimation

A. *Detection of Primary Synchronization Signal*

After post-compensation of the received signal, the UE tries to detect the 5G NR primary synchronization signal (PSS). For which, UE performs the cross-correlation in the time domain with (12) and 5G NR PSS $\mathbf{x}_{\mathrm{PSS}}^{(\iota)}[n]$ for all possible values of physical layer cell ID [20], $\iota = N_{\mathrm{ID}}^{(2)} \in \{0, 1, 2\}$, and selecting the value which maximizes the peak of cross-correlation given then the threshold. i.e

$$\hat{\iota} = \max_{\iota} \left\{ \sum_{i=0}^{N_{\mathrm{RX}}-1} \left| \mathbf{\Lambda}_{\iota,i}[k] \right| \right\} > \beta_{\mathrm{PSS}}, \forall\ \iota, \tag{13}$$

where $\mathbf{\Lambda}_{\iota,i}[k], \beta_{\mathrm{PSS}}$ denotes the cross-correlation in (14) and threshold evaluated for the desired probability of false alarm (15) respectively.

$$\mathbf{\Lambda}_{\iota,i}[k] = \sum_{n=0}^{N-1} \mathbf{x}_{\mathrm{PSS}}^{(\iota)}[n] \mathbf{y}_{c,p}^{(i)*}[n-k]. \tag{14}$$

However, the detector can falsely detect the PSS when the corresponding OFDM symbol does not contain PSS. Hence in the absence of PSS, the received signal is Gaussian noise, i.e., $\mathbf{y}_{c,p}^{(i)}[n] = \mathbf{w}_p^{(i)}[n]$. So the probability of a false alarm can be evaluated as

$$\begin{aligned} P_{\mathrm{FA}} &= \Pr\left\{ \sum_{i=0}^{N_{\mathrm{RX}}-1} \left| \mathbf{\Lambda}_{\iota,i}[k] \right| > \beta_{\mathrm{PSS}} \right\} \\ &= \Pr\left\{ Y > \beta_{\mathrm{PSS}} \right\} \\ &= 1 - F_Y(\beta_{\mathrm{PSS}}) \\ \beta_{\mathrm{PSS}} &= F_Y^{-1}(1 - P_{\mathrm{FA}}). \end{aligned} \tag{15}$$

where $Y = \sum_{i=0}^{N_{\mathrm{RX}}-1} \left| \mathbf{\Lambda}_{\iota,i}[k] \right|$. Fig. 4 shows our simulation; it has been verified that the random variable Y follows the Nakagami distribution, i.e., $Y \sim \mathrm{Nakagami}(m, \Omega)$, where m, Ω can be computed directly from the Y as, $m = (\mathbb{E}[Y^2])^2 / \mathbb{V}ar[Y^2]$ and $\Omega = \mathbb{E}[Y^2]$

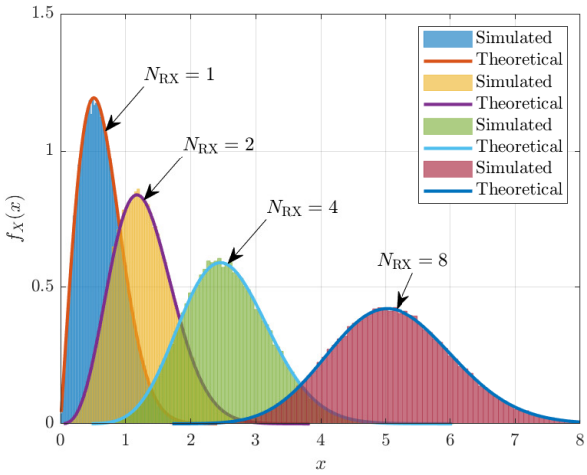

Fig. 4: Accuracy of distribution function

IV. Results and Discussions

In this section, we discuss the outcomes derived from the Monte Carlo simulations of our proposed method. Table I presents the simulation parameters. Furthermore, while introducing errors in trajectory and beam pointing, we have assumed that the mean of the random number will equal the actual value of the trajectory and beam pointing, respectively.

TABLE I: Simulation Parameters

Satellite Orbital Elements	Semimajor Axis, $\alpha = 6970000$ Eccentricity, $e = 0$ Inclination, $i = 0°$ RAAN, $\Omega = 0°$ Argument of periapsis, $\omega = 0°$ True Anomaly, $v = 0°$
Minimum elevation angle	$10°$
Beam center location	Latitude: -0.0010703823211031874 Longitude: 34.59977641558434
Frequency band	Ka-band
Carrier Frequency	$f_c = 20$ (GHz)
Minimum Bandwidth	28.8 (MHz)
Sub-carrier spacing	120 (kHz)
5G NR Downlink Signal	Synchronization Signal Block (SSB)
Tapped Delay Line	NTN TDL-D
Shadowing Standard Deviation	5 (dB)
Trajectory sphere standard deviation	$100, 1000, 10000$ (m)
Beam pointing standard deviation	$0.005°, 0.05°, 0.5°$
Probability of false alarm, P_{FA}	1/100

A. Maximum Residual Doppler Frequency

In this experiment, we assess the residual Doppler frequency due to errors in the trajectory sphere and beam pointing angle. In Fig. 5, it can be observed that the solid blue line corresponds to the ideal case, i.e., residual Doppler shift should be within half of the sub-carrier spacing for efficient estimation in an ideal scenario with zero errors. Moreover, from the simulation, it has been observed that the location of UE from the BC can be a maximum of up to 50 km. When we incorporate the errors, the residuals are close to the ideal scenario for the minor deviation. On the other hand, when the deviation is significant, the residual goes beyond the estimation bound. Nevertheless, the delay in satellite visibility is worth mentioning due to the increased separation of UE from the BC.

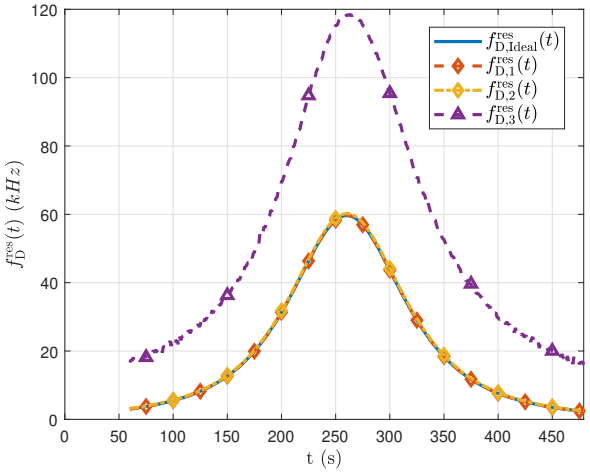

Fig. 5: Maximum residual Doppler frequency, where $f_{\text{D,1}}^{\text{res}}(t)$ = $(\sigma_{\ell,\text{sat}} = 100 \text{ m}, \sigma_{\theta_{\text{pc}}} = 0.005°)$ and $f_{\text{D,2}}^{\text{res}}(t)$ = $(\sigma_{\ell,\text{sat}} = 1000 \text{ m}, \sigma_{\theta_{\text{pc}}} = 0.05°)$, and $f_{\text{D,3}}^{\text{res}}(t)$ = $(\sigma_{\ell,\text{sat}} = 10000 \text{ m}, \sigma_{\theta_{\text{pc}}} = 0.5°)$

B. Root Mean Square Error of maximum residual Doppler frequency estimation

Here, we discuss the RMSE of normalized maximum residual Doppler frequency estimation versus SNR for the error in trajectory sphere and beam pointing. As from Fig. 5 it can be seen that for $\sigma_{\ell,\text{sat}} = 10000$ m, $\sigma_{\theta_{\text{pc}}} = 0.5°$ the maximum residual Doppler frequency is beyond the bound of estimation algorithm, we experiment for the remaining two errors as mentioned in Fig. fig:RMSE. It can be observed that error1 follows the ideal curve, whereas there is a slight deviation for error2. Nevertheless, this does not prevent the UE from detecting the PSS.

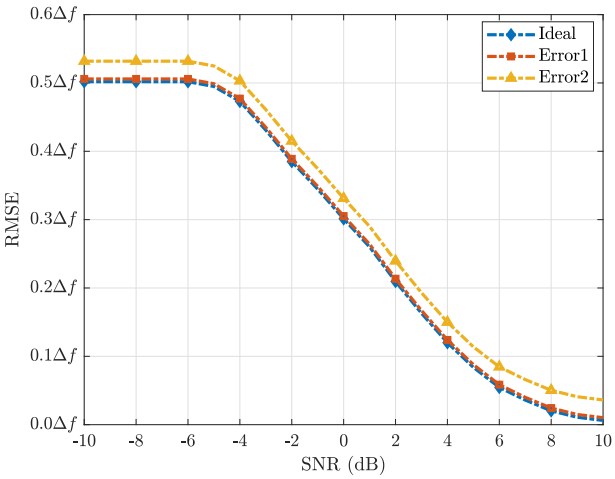

Fig. 6: Root mean square error of estimated residual Doppler frequency, where Error1 = $(\sigma_{\ell,\text{sat}} = 100 \text{ m}, \sigma_{\theta_{\text{pc}}} = 0.005°)$ and Error2 = $(\sigma_{\ell,\text{sat}} = 1000 \text{ m}, \sigma_{\theta_{\text{pc}}} = 0.05°)$

C. Probability of detection of PSS

This experiment investigated the 5G NR PSS detection probability for the maximum residual Doppler frequency versus SNR. It can be seen in Fig. 7, that even for the low SNR with an error in trajectory and beam pointing, the UE at a distance of 50 km from the BC attains a satisfactory probability equivalent to terrestrial 5G networks. It can further be improved by increasing the number of receive antennas.

V. Conclusion and Future Work

This paper describes an effective solution for mitigating the Doppler effect in a 5G NTN based on LEO. The method employs Doppler pre-compensation, eliminating the UE's need for satellite ephemeris during initial synchronization. Consequently, even in low SNR settings, the approach dramatically enhances the detection likelihood of PSS. Our analysis has shown that a deviation higher than 1km in the error trajectory and pointing error may lead to incorrect detection of PSS. The research suggests integer frequency offset estimation. Future research will examine scenarios with numerous spot beams serving UEs in various BC. This configuration, however, poses a problem at the edge, where interference from neighboring spot beam coverage may arise. To adequately manage this scenario, Joint Doppler and interference mitigation strategies will be required.

Acknowledgment

This work has been supported by the project TRANTOR, which has received funding from the European Union's Hori-

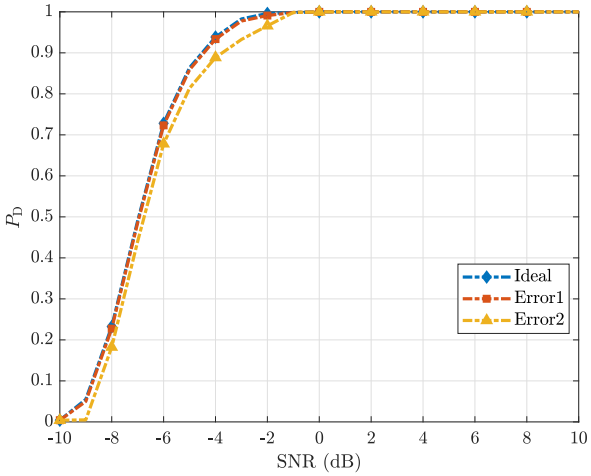

Fig. 7: Probability of detection of PSS, where Error1 = ($\sigma_{\ell,\text{sat}} = 100$ m, $\sigma_{\theta_{\text{pc}}} = 0.005°$) and Error2 = ($\sigma_{\ell,\text{sat}} = 1000$ m, $\sigma_{\theta_{\text{pc}}} = 0.05°$)

zon Europe research and innovation program under grant agreement No 101081983.

REFERENCES

[1] X. Lin, S. Rommer, S. Euler, E. A. Yavuz, and R. S. Karlsson, "5G from space: An overview of 3GPP Non-Terrestrial Networks," *IEEE Communications Standards Magazine*, vol. 5, no. 4, pp. 147–153, 2021.

[2] M. M. Azari, S. Solanki, S. Chatzinotas, O. Kodheli, H. Sallouha, A. Colpaert, J. F. Mendoza Montoya, S. Pollin, A. Haqiqatnejad, A. Mostaani, E. Lagunas, and B. Ottersten, "Evolution of non-terrestrial networks from 5G to 6G: A survey," *IEEE Communications Surveys Tutorials*, vol. 24, no. 4, pp. 2633–2672, 2022.

[3] F. Rinaldi, H.-L. Maattanen, J. Torsner, S. Pizzi, S. Andreev, A. Iera, Y. Koucheryavy, and G. Araniti, "Non-terrestrial networks in 5G & beyond: A survey," *IEEE access*, vol. 8, pp. 165 178–165 200, 2020.

[4] P. Moose, "A technique for orthogonal frequency division multiplexing frequency offset correction," *IEEE Transactions on Communications*, vol. 42, no. 10, pp. 2908–2914, 1994.

[5] "3GPP TR 38.821, "3rd generation partnership project; technical specification group radio access network; solutions for NR to support non-terrestrial networks (NTN) (release 16)," 2021.

[6] I. Ali, N. Al-Dhahir, and J. Hershey, "Doppler characterization for LEO satellites," *IEEE Transactions on Communications*, vol. 46, no. 3, pp. 309–313, 1998.

[7] J. Lin, Z. Hou, Y. Zhou, L. Tian, and J. Shi, "MAP estimation based on doppler characterization in broadband and mobile LEO satellite communications," in *2016 IEEE 83rd Vehicular Technology Conference (VTC Spring)*, 2016, pp. 1–5.

[8] A. Guidotti, A. Vanelli-Coralli, M. Caus, J. Bas, G. Colavolpe, T. Foggi, S. Cioni, A. Modenini, and D. Tarchi, "Satellite-enabled LTE systems in LEO constellations," in *2017 IEEE International Conference on Communications Workshops (ICC Workshops)*, 2017, pp. 876–881.

[9] W. Wang, Y. Tong, L. Li, A.-A. Lu, L. You, and X. Gao, "Near optimal timing and frequency offset estimation for 5G integrated LEO satellite communication system," *IEEE Access*, vol. 7, pp. 113 298–113 310, 2019.

[10] M. Conti, S. Andrenacci, N. Maturo, S. Chatzinotas, and A. Vanelli-Coralli, "Doppler impact analysis for NB-IoT and satellite systems integration," in *ICC 2020 - 2020 IEEE International Conference on Communications (ICC)*, 2020, pp. 1–7.

[11] M. Huang, J. Chen, and S. Feng, "Synchronization for OFDM-based satellite communication system," *IEEE Transactions on Vehicular Technology*, vol. 70, no. 6, pp. 5693–5702, 2021.

[12] D. Nieto Yll, "Doppler shift compensation strategies for LEO satellite communication systems," Ph.D. dissertation, UPC, Escola Tècnica Superior d'Enginyeria de Telecomunicació de Barcelona, Departament de Teoria del Senyal i Comunicacions, Jun 2018. [Online]. Available: http://hdl.handle.net/2117/123510

[13] D. Tian, Y. Zhao, J. Tong, G. Cui, and W. Wang, "Frequency offset estimation for 5G based LEO satellite communication systems," in *2019 IEEE/CIC International Conference on Communications in China (ICCC)*, 2019, pp. 647–652.

[14] M. Pan, J. Hu, J. Yuan, J. Liu, and Y. Su, "An efficient blind doppler shift estimation and compensation method for LEO satellite communications," in *2020 IEEE 20th International Conference on Communication Technology (ICCT)*, 2020, pp. 643–648.

[15] J. Wang, C. Jiang, L. Kuang, and B. Yang, "Iterative doppler frequency offset estimation in satellite high-mobility communications," *IEEE Journal on Selected Areas in Communications*, vol. 38, no. 12, pp. 2875–2888, 2020.

[16] X. Lin, Z. Lin, S. E. Löwenmark, J. Rune, R. Karlsson, and Ericsson, "Doppler shift estimation in 5G new radio non-terrestrial networks," in *2021 IEEE Global Communications Conference (GLOBECOM)*, 2021, pp. 1–6.

[17] S. Kumar, A. Astro, O. Kodheli, J. Querol, S. Chatzinotas, T. Schlichter, G. Casati, T. Heyn, F. Völk, S. Kaya *et al.*, "5G-NTN GEO-based in-lab demonstrator using openairinterface5G," in *11th Advanced Satellite Multimedia Conference*, 2022.

[18] S. Kumar, A. K. Meshram, A. Astro, J. Querol, T. Schlichter, G. Casati, T. Heyn, F. Völk, R. T. Schwarz, A. Knopp *et al.*, "Openairinterface as a platform for 5G-NTN research and experimentation," in *2022 IEEE Future Networks World Forum (FNWF)*. IEEE, 2022, pp. 500–506.

[19] "3GPP TR 38.811, "3rd generation partnership project; technical specification group radio access network; study on new radio (NR) to support non-terrestrial networks (release 15)," 2020-09.

[20] "3GPP TS 38.211, "NR; Physical channels and modulation." 3rd Generation Partnership Project; Technical Specification Group Radio Access Network. (release 17.4.0)," 2023-01.

[21] J. van de Beek, M. Sandell, and P. Borjesson, "Ml estimation of time and frequency offset in OFDM systems," *IEEE Transactions on Signal Processing*, vol. 45, no. 7, pp. 1800–1805, 1997.